Desalination and Water Treatment
www.deswater.com
doi: 10.5004/dwt.2022.29017

278 (2022) 195–208
December

Response surface methodology for removal of methyl violet dye using *Albizia stem bark Lebbeck* modified by $Fe_2(MoO_4)_3$ nanocomposite from aqueous solutions and assessment relative error by neural network model

Shiva Einolghozati[a], Elham Pournamdari[b,*], Nasrin Choobkar[a], Farzaneh Marahel[c]

[a]*Department of Environment, Kermanshah Branch, Islamic Azad University, Kermanshah, Iran, emails: Shiva_einolghozati67@yahoo.com (S. Einolghozati), Nchoobkar20@gmail.com (N. Choobkar)*
[b]*Department of Chemistry, Islamshahr Branch, Islamic Azad University, Islamshahr, Iran, email: elhampurnamdari@gmail.com*
[c]*Department of Chemistry, Omidiyeh Branch, Islamic Azad University, Omidiyeh, Iran, email: Farzane.marahel.fm@gmail.com*

Received 19 April 2022; Accepted 10 October 2022

ABSTRACT

The applicability of *Albizia stem bark Lebbeck* modified by $Fe_2(MoO_4)_3$ nanocomposite, was studied for eliminating methyl violet dye from aqueous solutions. Identical techniques including (infrared, X-ray diffraction, and scanning electron microscopy) have been utilized to characterize this novel material. The impacts of variables including initial methyl violet concentration (X_1), pH (X_2), adsorbent dosage (X_3), and sonication time (X_4) came under scrutiny using central composite design under response surface methodology. The values of 20 mg L^{-1}, 0.03 g, 5.0, 3.0 min were considered as the ideal values for methyl violet concentration, adsorbent, pH, and contact time, respectively. Adsorption equilibrium and kinetic data were fitted with the Langmuir monolayer isotherm model and pseudo-second-order kinetics (R^2: 0.999) with maximum adsorption capacity (120.4 mg g^{-1}), respectively. Thermodynamic parameters ($\Delta G°$: –9.26 kJ mol^{-1}, $\Delta H°$: –29.24 kJ mol^{-1}, $\Delta S°$: –131.49 kJ mol^{-1} K^{-1}), also indicated methyl violet adsorption is feasible, spontaneous and exothermic. The observed outcome is the suitability of the artificial neural network model as a tool for mean square error (ANN = 0.190, and FL = 0.3397), for the removal of methyl violet dye. Overall results confirmed that *Albizia stem bark Lebbeck* modified by $Fe_2(MoO_4)_3$ nanocomposite is an effective adsorbent for removing the dyes from an aqueous solutions.

Keywords: Methyl violet dye; Adsorption; Isotherms; Central composite design; Response surface methodology; Neural network model

1. Introduction

The severity of water pollution has resulted from the economic development adopted by humans overall in the worldwide. Industries consume vast quantities of water and generate an enormous amount of impurities, including dyes, detergents, additives, suspended solids, aldehydes, heavy metals, non-biodegradable matter, and insoluble substances [1]. Wastewaters of industries like textile, paper, rubber, plastic, leather, cosmetic, food, and drug contain dyes, and pigments that are hazardous, and can cause skin irritation, and cancer due to the colorization of the water [2,3]. During the past few years, there has been an increasing concern regarding the residual dye in textiles, as it will be released into the environment, and resist aerobic and anaerobic conditions, heat, light, and oxidation. Residual dye is produced when an incomplete or excess of dyes onto textile fiber is incoming out during an aqueous dyeing and washing process [4]. Therefore, it is necessary to remove toxic dyes is required to safeguard human and eco-system health from industrial wastewater [5].

* Corresponding author.

Methyl violet (MV), is a basic dye, with high brilliance and intensity and is highly used in the industry. The seen show structured (MV) dye in Fig. 1 [6,7]. Also, ingestion, inhalation, skin contact, and long-term exposure can cause eye and skin damage [8]. The harmful properties of (MV) dye create urgency from industrial wastewater before being discharged into the environment [9]. Various treatment methods must remove dyes from contaminated wastewater, including advanced oxidation processes, catalytic degradation, and adsorption. An adsorption is a promising approach owing to its simple operational design, non-susceptibility to pollutants, reusability, high efficiency, low cost, and relatively low waste production [10,11].

The adsorption method is especially suitable for solving dyes, environmental, gases, and metals problem, and has many advantages, so it has become the focus and hot spot of research. In comparison with other conventional techniques (ion exchange, biological treatments, and electrolysis), adsorption is one of the most successful and uncomplicated techniques for deletion of toxic and noxious contaminations. Its popularity is due to advantages including higher efficiency lower waste, facile, and mild operational conditions. The successfulness of adsorption techniques in deletion of pollutants especially those which are extremely stable in biological degradation process via economically accomplishable mild ways [12–18]. Thus, the extensive utilization of adsorption techniques for deletion of numerous chemicals from aqueous solutions seems logical [17,18]. In recent years, it has been tried to eliminate specified organics from water samples by applying various potential adsorbents. In this regard, magnetic nanoparticles (MNPs) have been studied extensively as novel adsorbents with large surface area, high adsorption capacity and small diffusion resistance. For instance, they have been used for the separation of chemical species such as environmental pollutants, metals, dyes, and gases [19,20]. Iron oxide nanoparticles are widely used for metal remediation due to their low toxicity and easy separation from water media in addition, where the nanoparticle (NP) is composed of magnetite, a facile magnetic separation of NPs, along with associated contaminants, can be performed. However, bare magnetite nanoparticles rapidly aggregate in aqueous systems and are highly susceptible to transformations under many environmental conditions [21–24].

An artificial neural network model is a numerical estimation technique, which to find nonlinear relationships between input and output variables. Various topics, such as modeling wastewater and aqueous solutions. This work was to evaluate the use of an artificial neural network model to predict the (MV) dye removal from wastewater by *Albizia stem bark Lebbeck* modified by $Fe_2(MoO_4)_3$ nanocomposite [4,24,25]. The experimental conditions of pH of the solution, contact time, initial (MV) dye concentration, adsorbent dosage, and the dye removal percentage, were investigated and optimized by central composite design (CCD) under response surface methodology (RSM). The adsorption of (MV) dye follows the pseudo-second-order rate equation, and Langmuir's model for the equilibrium data explanation. The capability of *Albizia stem bark Lebbeck* modified by $Fe_2(MoO_4)_3$ nanocomposite in eliminating (MV) dye from aqueous solutions was demonstrated by evidence.

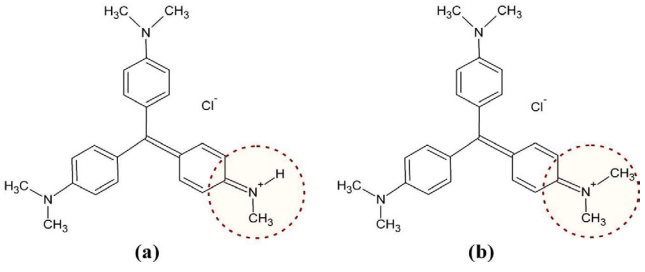

Fig. 1. Structures of methyl violet (MV) dye: (a) 2B and (b) 10B.

2. Experimental

2.1. Materials and instrumentation

All the chemicals used are of the highest purity and purchased from Merck (Darmstadt, Germany). Methyl violet dye (98%), ammonium heptamolybdate (99%), and iron nitrate(III) (98.0%). The applied instruments were as follow: spectrophotometer model 1601 PC (Shimadzu Company, Japan). Infrared (IR) (Spectra model, PerkinElmer Company, Germany). Scanning electron microscopy (SEM; Phillips model, PW3710, Netherland), was used to study the morphology of samples. An ultrasonic bath with a heating system (Tecno-GAZ SPA Ultra Sonic System, Italy), was used for the ultrasound-assisted adsorption procedure.

2.2. Preparation of Albizia stem bark Lebbeck

The *Albizia stem bark Lebbeck* powder, this material, is a zero-value agricultural waste product. The off woody of the *Albizia stem bark Lebbeck* powder plant, thoroughly washed with water, and sun-dried for 5 d. The dried biomass was milled and then fractionated using 100–300 m analytical sieves and washed twice with 0.01 M HCl to remove any dyes on the biomass [26].

2.3. Preparation of Albizia stem bark Lebbeck modified by $Fe_2(MoO_4)_3$ nanocomposite

The iron oxide-molybdenum nanocomposite was prepared in a synergistic process by mixing the juice solutions of heptamolybdate ammonium and iron nitrate mode as follows: The container with the heptamolybdate ammonium was placed, in a warm bath with a temperature of 70°C, and the iron nitrate solution was added slowly while stirring the ammonium heptamolybdate solution. Then we increased the bath temperature to 90°C. The sediment suspension was stirred for 3 h. Stirring was stopped and the suspension was placed in the laboratory for 2 h. The *Albizia stem bark Lebbeck* modified by $Fe_2(MoO_4)_3$ nanocomposite produced suspensions were prepared from a leaf medlar with an equal weight ratio and after analysis, Brunauer–Emmett–Teller (BET), IR, X-ray diffraction (XRD) and SEM were used as adsorbent [26,27].

2.4. Adsorption experiments

Generally, the sonochemical adsorption experiment was carried out in a batch mode as follows: The Erlenmeyer

flask was loaded with exact quantities of (MV) dye solution (50 mL) at a specified concentration of 20 mg L^{-1} and pH of 5.0 with a known quantity of adsorbent (0.03 g), while the desired sonication time (3 min) was maintained at 25°C. The adsorption trials were executed in mode, and the solution was ultrasonicated at conditions devised under RSM. At the end of the adsorption process, the sample solution was immediately centrifuged and the analysis of the dilute phase was done for determining (MV) dye concentration with the help of UV–Vis spectrophotometer at a wavelength of 580 nm, as shown in Fig. 2. The equilibrium concentrations and removal efficiency (%) of the (MV) dye were calculated according to Eqs. (1) and (2), respectively. All experiments five times, and final results were presented as mean values.

$$R\% = \frac{C_0 - C_e}{C_0} \times 100 \quad (1)$$

$$q_i = \frac{V\left(C_0 - C_e\right)}{M} \times 100 \quad (2)$$

where C_0 (mg L^{-1}) in the formula refers to the initial (MV) dye concentration, and C_e (mg L^{-1}) represents the equilibrium (MV) dye concentration in an aqueous solution. V (L) shows the solution volume, and W (g) signifies the mass adsorbent [28].

2.5. Central composite design

The central composite design, for modeling, and the optimization of the effects of concentration of (MV) dye (X_1), pH (X_2), amount of adsorbent (X_3), and contact time (X_4) on the ultrasonic-assisted adsorption of MV dye by *Albizia stem bark Lebbeck* modified by $Fe_2(MoO_4)_3$ nanocomposite. Four levels at which the R% of (MV) dye as a response was determined and shown in Tables 1 and 2. To evaluate the essential, and effective terms for modeling the answer based on F-test. P-values less than 0.05 are generally considered a criterion for distinguishing statistically significant variables [28,29].

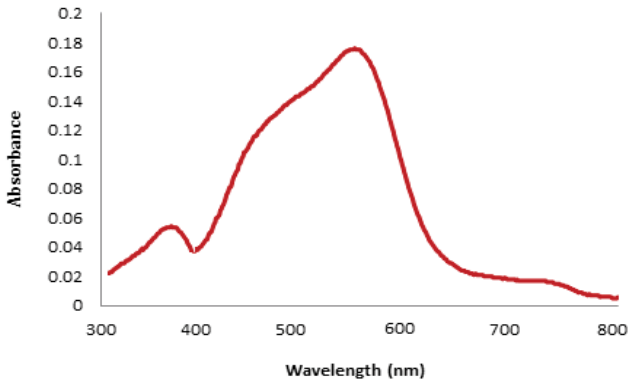

Fig. 2. Absorption spectra of (MV) dye onto *Albizia stem bark Lebbeck* modified by $Fe_2(MoO_4)_3$ nanocomposite.

Table 2
Design and the response

Run	X_1	X_2	X_3	X_4	R% (MV) dye
1	10	5	0.030	3	100.0
2	10	4	0.025	4	95.0
3	15	5	0.03	3	99.1
4	10	6	0.025	4	94.0
5	20	6	0.015	5	90.4
6	10	5	0.035	2	100.0
7	10	7	0.025	6	95.0
8	15	8	0.025	4	96.0
9	15	6	0.025	4	95.0
10	15	6	0.015	4	100.0
11	20	7	0.025	6	95.0
12	10	5	0.035	2	96.0
13	15	6	0.025	4	100.0
14	15	6	0.025	4	93.0
15	10	5	0.015	6	81.8
16	15	6	0.025	4	76.8
17	20	5	0.015	6	96.5
18	15	6	0.005	4	100.0
19	20	5	0.015	2	80.0
20	10	7	0.035	2	92.5
21	20	5	0.015	2	95.0
22	20	6	0.035	2	99.2
23	15	6	0.025	4	97.5
24	10	5	0.035	4	100.0
25	15	5	0.025	6	95.0
26	10	4	0.015	6	96.0
27	5	6	0.025	4	77.7
28	10	4	0.015	6	97.7
29	10	5	0.035	4	99.1
30	15	7	0.025	2	95.0

Table 1
Experimental factors, levels, and matrix of CCD

Factors	Symbol	Levels			Star point α = 2.0	
		Low (–1)	Central (0)	High(+1)	–α	+α
Conc. (MV) dye (mg L^{-1})	(X_1)	10.0	15.0	20.0	5.0	25.0
pH	(X_2)	2.0	5.0	6.0	4.0	8.0
Conc. sorbent (g)	(X_3)	0.015	0.025	0.03	0.075	0.035
Time (min)	(X_4)	2.0	3.0	4.0	2.0	6.0

2.6. Artificial neural network

In recent years in different fields of science, various applications of artificial neural network models were provided. Therefore, the application of intelligent systems, including the use of artificial neural network, is expanding to model complex systems. The artificial neural network can accurately describe complex and nonlinear relationships with precise rules. Due to the high accuracy, the artificial neural network is one of the best tools to predict the results of processes using laboratory data. Similar studies confirm this fact. In this research, modeling by MATLAB software. To identify this model, also we must introduce our data to software in normalized view [30].

In the network, neurons are in several layers. These layers are the input layer, a hidden layer or layers (middle), and (MLP), a layer of perceptron, multilayer outputs. Each neuron to all neurons in the next layer, but there are no connections between neurons in one layer. A model artificial neural network (ANN) with four input layers (initial (MV) dye concentration, *Albizia stem bark Lebbeck* modified by $Fe_2(MoO_4)_3$ nanocomposite dosage, pH, and time), were detected at epoch numbers 50, and 32 experimental points to feed of the model were employed. Mean squared error (MSE), based on the function, error performance function showed a minimum value of five neurons. Data points in the training, test, and validation sets contained 70%, 15%, and 15%, respectively, and the data set was derived. In the present study, Levenberg–Marquardt backpropagation algorithm the network [31,32].

This algorithm: All samples were normalized between 0–1, to achieve fast convergence, commensurability of the scale of the input, as well as the minimal R_{MSE} values. The normalized values of data according to Eq. (3):

$$X_{norm} = \frac{X - X_{min}}{X_{max} - X_{min}} \tag{3}$$

where X is a variable, but X_{min} and X_{max} refer to the minimum value and the maximum value, respectively. Statistical parameters: correlation coefficient (R^2), the mean squared error (MSE), total squared error (SSE), and standard deviation (SD) are calculated through Eqs. (4)–(7), respectively [30–32].

$$R^2 = \frac{\sum\left(Y_{exp,i} - Y_{model,mean}\right)^2 - \sum\left(Y_{model,i-Y_{exp,i}}\right)^2}{\sum\left(Y_{exp,i} - Y_{model,mean}\right)^2} \tag{4}$$

$$MSE = \frac{\sum\left(Y_{model,i} - Y_{exp,i}\right)^2}{n} \tag{5}$$

$$SSE = \sum\left(Y_{model,i} - Y_{exp,i}\right)^2 \tag{6}$$

$$SD = \sqrt{\frac{1}{n-1}\sum\left(\left|\frac{Y_{exp,i} - Y_{model,i}}{Y_{exp,i}}\right| - AARE\right)^2} \tag{7}$$

3. Results and discussion

3.1. Characterization of adsorbent

3.1.1. BET; analysis of Albizia stem bark Lebbeck modified by $Fe_2(MoO_4)_3$ nanocomposite

The nitrogen adsorption–desorption isotherm at 77 K onto *Albizia stem bark Lebbeck* modified by $Fe_2(MoO_4)_3$ nanocomposite is presented in Fig. 3. The adsorption capacity with an increase in the number of adsorbed $Fe_2(MoO_4)_3$ nanocomposite, the relative partial pressure range on the adsorption isotherms gradually decreases. Because the $Fe_2(MoO_4)_3$ nanocomposite, in the composite spread into *Albizia stem bark Lebbeck* channels, made the channels, narrow and the pore volume decrease. By comparing the pore size distribution of the samples, it can be that with the increase in the adsorbed $Fe_2(MoO_4)_3$ nanocomposite, the most probable pore diameter. Because, when the $Fe_2(MoO_4)_3$ nanocomposite, was introduced into the *Albizia stem bark Lebbeck* channels, the most probable pore diameter reduced, indicating that the $Fe_2(MoO_4)_3$ nanocomposite, entered the *Albizia stem bark Lebbeck* channels, shown in Table 3 [33].

3.1.2. IR, XRD, and energy-dispersive X-ray spectroscopy analysis

The IR spectra of *Albizia stem bark Lebbeck* and *Albizia stem bark Lebbeck* modified by $Fe_2(MoO_4)_3$ nanocomposite in the 500–4,000 cm^{-1} wave number range, as demonstrated in (Fig. 4a). While the broad signals at 1,016.45–1,059.99 cm^{-1} is ascribable to C–H stretching from phenolic and alcoholic groups, the one at 776.5 cm^{-1} is attributable to Fe–O. Also the apparent signals at 3,101.21 and 3,418.89 cm^{-1} are attributable to C–OH stretching [26,27]. Fig. 4b represents the X-ray diffraction of the *Albizia stem bark Lebbeck* modified by $Fe_2(MoO_4)_3$ nanocomposite adsorbent. The peaks at at 2θ = 21.45°, 33.0°, 37.2°, 44.75°, 56.0° and 62.0° belong to the lattice planes of at (111), (220), (311), (400), (440), and (511), confirming the cubic structure of *Albizia stem bark Lebbeck* modified by $Fe_2(MoO_4)_3$ nanocomposite. However the great intensity of signal at 37.2° (311) confirmed that there is a slight amount of amorphous state material. Indeed, the

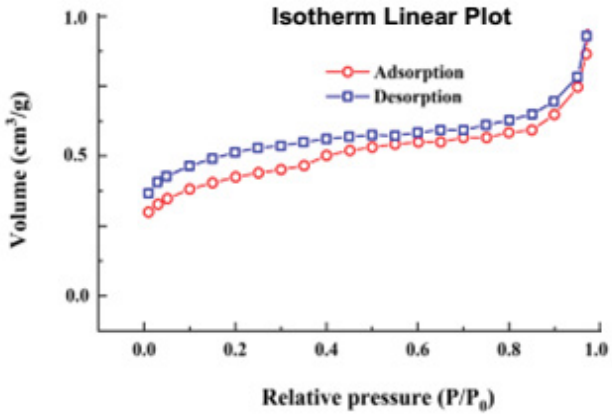

Fig. 3. N_2 gas adsorption/desorption isotherms of *Albizia stem bark Lebbeck* and *Albizia stem bark Lebbeck* modified by $Fe_2(MoO_4)_3$ nanocomposite.

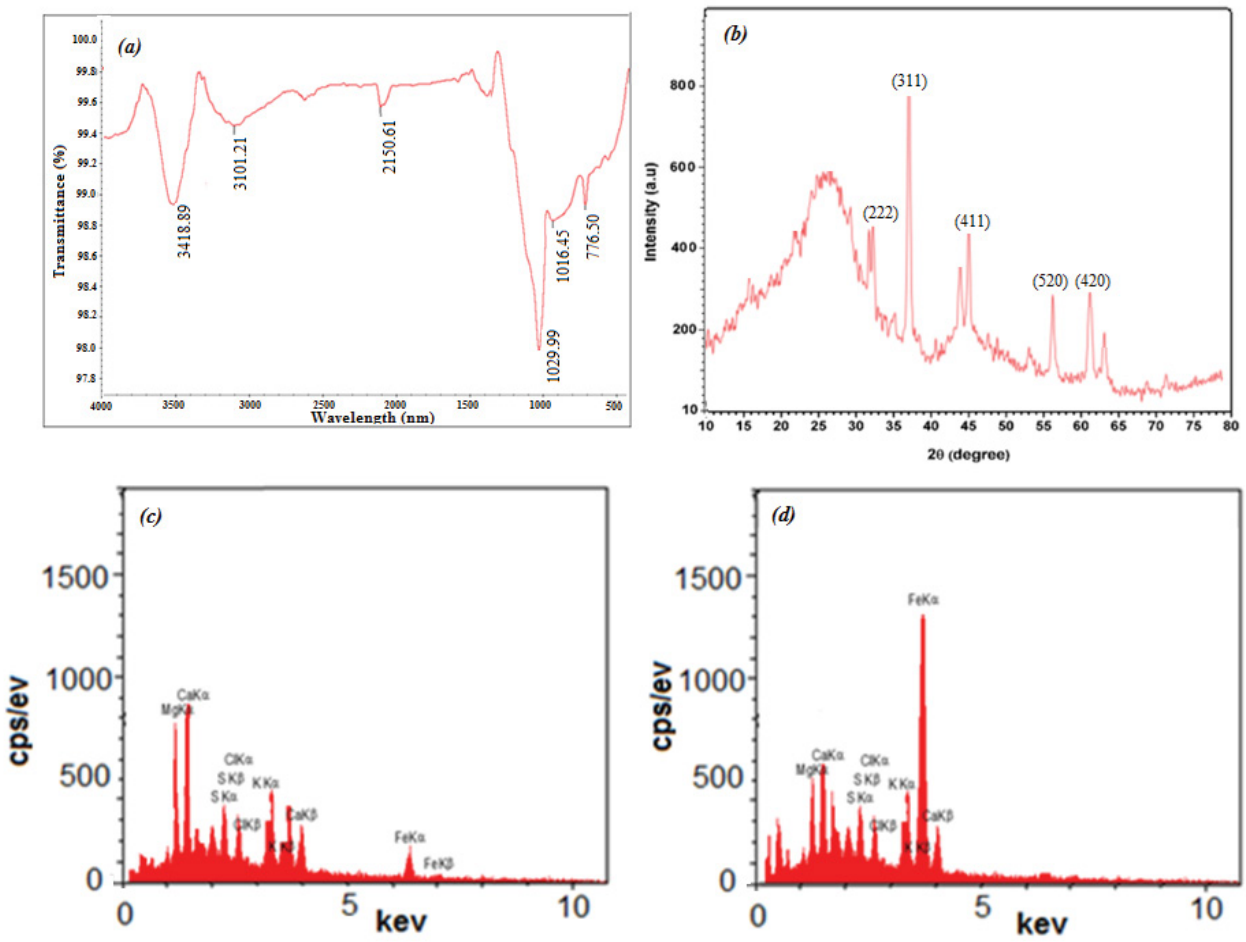

Fig. 4. (a) The infrared of the developed *Albizia stem bark Lebbeck* modified by $Fe_2(MoO_4)_3$ nanocomposite, (b) XRD of the prepared of *Albizia stem bark Lebbeck* modified by $Fe_2(MoO_4)_3$ nanocomposite, (c) EDX spectrum of prepared *Albizia stem bark Lebbeck*, and (d) EDX spectrum of prepared *Albizia stem bark Lebbeck* modified by $Fe_2(MoO_4)_3$ nanocomposite.

perfect synthesis of MgO-SiO_2 NPs can be judged through looking at its XRD pattern [34]. The energy-dispersive X-ray spectroscopy (EDX) spectrum of *Albizia stem bark Lebbeck* is exhibited in Fig. 4c. It is worthy of note that, functionalized *Albizia stem bark Lebbeck* modified by $Fe_2(MoO_4)_3$ nanocomposite became uneven. In Fig. 4d, the EDX spectrum of *Albizia stem bark Lebbeck* modified by $Fe_2(MoO_4)_3$ nanocomposite is shown [34,35].

3.1.3. Surface morphology

The morphological properties of *Albizia stem bark Lebbeck* modified by $Fe_2(MoO_4)_3$ nanocomposite was investigated by SEM and is exhibited in Fig. 5. The evenness, homogeneity, orderliness and approximate uniformity of synthesized *Albizia stem bark Lebbeck* modified by $Fe_2(MoO_4)_3$ nanocomposite (even in size distribution) can be observed. *Albizia stem bark Lebbeck* modified by $Fe_2(MoO_4)_3$ nanocomposite after surface modification came to be uneven, bigger and agglomerate. It can be seen that the particles are mostly spherical with the various size distribution as they form agglomerates. Based on the particles size distribution, we obtained the average particle size in the range of 40–60 nm very close to those determined by XRD analysis [32].

3.2. Point-of-zero charge

The adsorption mechanism of (MV) dye is better understood by determination of surface charge of the adsorbent which is determined from the potential zeta study. The Point (pH_{pzc}), variation is shown in Fig. 6. This value indicates that the sorbent surface can acquire a positive charge at pH < pH_{pzc}. By contrast, the surface charge of the sorbent is negative at the solution pH of 5, indicating the capability of (MV) dye adsorption onto *Albizia stem bark Lebbeck* modified by $Fe_2(MoO_4)_3$ nanocomposite. The pH value of the solution affects the surface charge of the adsorbent and the uptake behavior and efficiency of the adsorbent as shown in Fig. 6 [36].

3.3. A comparative study

The adsorption percent of MV dye onto each of $Fe_2(MoO_4)_3$ NPs, *Albizia stem bark Lebbeck*, and *Albizia*

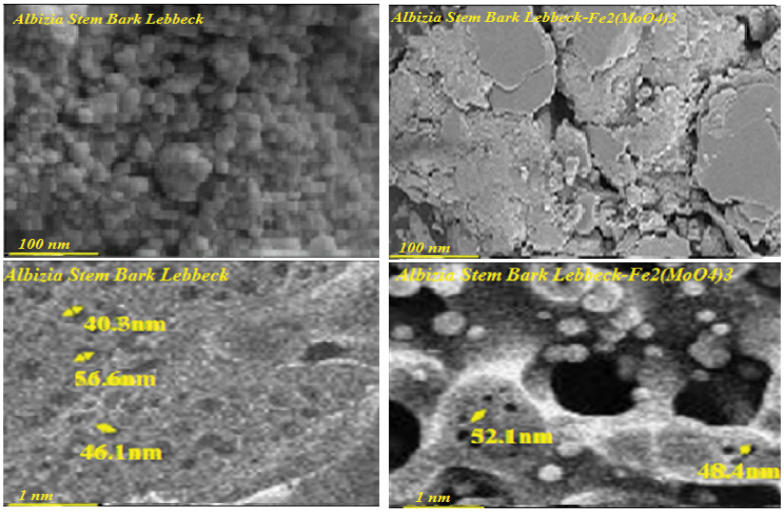

Fig. 5. SEM image of the prepared *Albizia stem bark Lebbeck* modified by $Fe_2(MoO_4)_3$ nanocomposite in 100 and 1 nm.

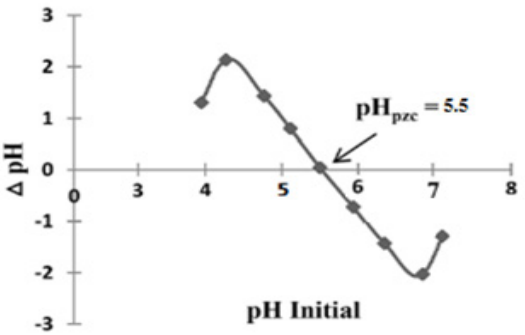

Fig. 6. pH_{pzc} of the (MV) dye in solution.

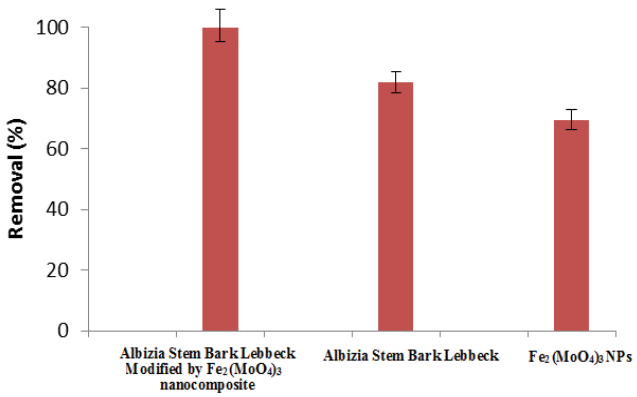

Fig. 7. Comparison of the effectively of $Fe_2(MoO_4)_3$ NPs, *Albizia stem bark Lebbeck* and *Albizia stem bark Lebbeck* modified by $Fe_2(MoO_4)_3$ nanocomposite [C_0 = 20.0 mg L^{-1}; pH = 5.0; dosage sorbent = 0.03 g; time = 3.0 min].

stem bark Lebbeck modified by $Fe_2(MoO_4)_3$ nanocomposite at the optimum condition, and the obtained results in Fig. 7 [5,28]. As can see, the trend of the effectiveness of mentioned adsorbents for removing MB from aqueous media is as follows: *Albizia stem bark Lebbeck* modified by $Fe_2(MoO_4)_3$ nanocomposite (99.2%) > *Albizia stem bark Lebbeck* (83.7.0%) > $Fe_2(MoO_4)_3$ NPs (71.4%).

3.4. Modeling process

Analyzing accurate data from the RSM is another practical application of Design-Expert STATISTICA 10.0 software. RSM is a statistical method used to perform experiment analysis, modeling, and process optimization. In an RSM model, the response variable (Y) is affected by several independent variables (X_1, X_2, X_3, and X_n). RSM, the most complex model is the second-order or quadratic model, which includes the relationship between response and independent variables (contains components such as first power, interactive impacts, polynomial function, and intercept point). The quadratic model by Eq. (8) [36,37].

$$\begin{aligned} R\%(\mathrm{MV})\,\mathrm{dye} = {} & 95.709 - 2.1767X_1 - 1.0258X_2 \\ & + 0.94833X_3 + 6.3233X_4 + 2.0955X_5 \\ & - 1.4350X_1X_2 + 1.3388X_1X_3 + 2.9638X_1X_4 \\ & - 1.1638X_1X_5 + 0.69000X_2X_3 + 1.0650X_2X_4 \\ & - 1.3900X_2X_5 - 1.6612X_3X_4 + 1.4612X_3X_5 \\ & - 1.9138X_4X_5 + 0.66726X_1^2 + 0.91726X_2^2 \\ & - 0.020244X_3^2 - 2.8327X_4^2 - 0.41595X_5^2 \end{aligned} \quad (8)$$

The value of the determination coefficient for deleting (MV) dye in Table 4, it has been noticed that the response surface quadratic model was a befitting model for predicting the function of (MV) dye adsorption on *Albizia stem bark Lebbeck* modified by $Fe_2(MoO_4)_3$ nanocomposite.

3.5. RSM analysis

Response surface methodology (RSM) was utilized to ameliorate the optimization and estimation of all significance interaction of variables and the relative significance of adsorption processes. Fig. 8 exhibits the

Table 3
Characterization analysis BET of sorbent

Characterization		Samples	
		Albizia stem bark Lebbeck	*Albizia stem bark Lebbeck* modified by $Fe_2(MoO_4)_3$
BJH desorption	Correlation coefficient	0.9972	0.9915
	Surface area ($m^2\ g^{-1}$)	45.84	45.17
	Pore volume ($cm^3\ g^{-1}$)	0.9202	0.8917
BJH adsorption	Surface area ($m^2\ g^{-1}$)	90.27	89.80
	Pore volume ($cm^3\ g^{-1}$)	0.9493	0.9288

Table 4
Analysis of variance for the full quadratic model

Source of variation	DF	(MV) dye			
		Sum square	Mean square	*F*-value	*P*-value
Model	14	3,105	157.8	22.89	<0.0001
X_1	1	151.68	151.68	23.64	0.00054
X_2	1	793.2	793.2	112.3	<0.0001
X_3	1	13.87	13.87	2.2	<0.0001
X_4	1	31.98	31.98	4.638	0.1705
X_1X_2	1	74.512	74.512	8.78	0.051
X_1X_3	1	33.015	33.015	3.88	0.0476
X_1X_4	1	202.18	202.18	486.87	0.0002
X_2X_3	1	12.78	12.78	31.044	<0.0001
X_2X_4	1	0.486	0.486	1.1849	0.0105
X_3X_4	1	3.102	3.102	7.521	0.015031
X_3X_5	1	225.63	225.63	545.16	<0.0001
X_1^2	1	24.53	24.53	2.85	0.11233
X_2^2	1	0.012118	0.012118	0.001389	0.0105
X_3^2	1	234.02	234.02	27.196	0.0178
X_4^2	11	8.330	8.330	1.259	0.2849
Residual	5	72.78	6.611		
Lack of fit	6	44.05	7.433	1.278	0.3982
Pure error	31	28.86	5.737		
Cor. total		3082			

three-dimensional surface response plots of this interaction. The plots were prepared for a specified pair of factual factors at optimal and fixed values of other variables [37,38]. A positive increase in the (MV) dye removal percentage with the increase in adsorbent mass. Significant diminish in removal percentage of the lower amount of *Albizia stem bark Lebbeck* modified by $Fe_2(MoO_4)_3$ nanocomposite is attributed to the higher ratio of (MV) dye molecules to the vacant sites of the adsorbent. Maximum (MV) dye deletion of 100%, the optimum conditions were as follows: pH of 5.0, ultrasound time of 3.0 min, the adsorbent mass of (0.03 g), and initial (MV) dye equal to 20.0 mg L^{-1}, for (MV) dye. Based on the excellent conformity between the experimental and prediction data, successfully for the evaluation and optimization of the influences of the adsorption independent variables on the removal efficiency of (MV) dye from aqueous media with the help of *Albizia stem bark Lebbeck* modified by $Fe_2(MoO_4)_3$ nanocomposite [39,40].

3.6. Optimization of CCD

The profile for desirable option with the predicted values in the STATISTICA 10.0 software was used for the optimization of the process shown in Fig. 9. Based on the excellent conformity between the experimental and prediction data, successfully for the evaluation and optimization of the influences of the adsorption independent variables

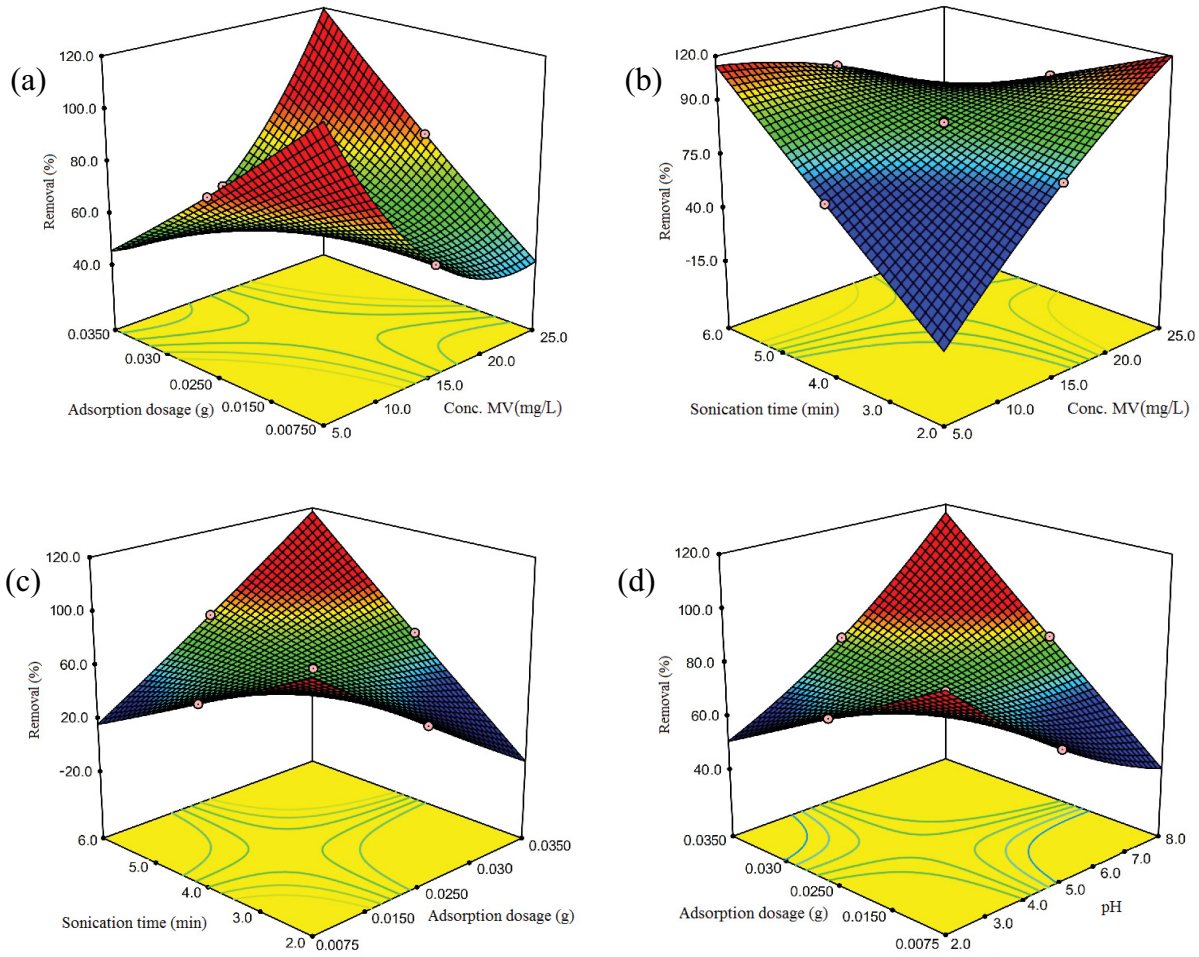

Fig. 8. Response surfaces for the dye removal: (a) adsorbent dosage – initial (MV) dye concentration, (b) contact time, initial (MV) dye concentration, (c) contact time – adsorbent dosage, and (d) (MV) dye adsorbent dosage (MV) dye – pH.

on the removal efficiency of (MV) dye from aqueous media with the help of *Albizia stem bark Lebbeck* modified by $Fe_2(MoO_4)_3$ nanocomposite [37,38].

3.7. Modeling of the artificial neural network process

In Figs. 10 and 11, the plots of errors histogram for the adsorption processes, are demonstrated, indicating that the errors in this removal process are low. The net training process in this study, the MSE based on the function of error [30,31]. This method with four input layers (viz., initial (MV) dye concentration, *Albizia stem bark Lebbeck* modified by $Fe_2(MoO_4)_3$ nanocomposite dosage, pH, and time) based on the output layers (determining of target compounds) as shown in Table 5. The performance of the neuro-fuzzy logic model (FL), and artificial neural network model (ANN) in predicting the separation percentage is much better and very similar and close to the actual data, and the results are excellent and acceptable. Indicates that the neuro-fuzzy logic model (FL), and artificial neural network model (ANN) have the lowest mean error and the highest value of correlation coefficient for removal of the (MV) dye onto *Albizia stem bark Lebbeck* modified by $Fe_2(MoO_4)_3$ nanocomposite. The mean square error of 0.19 for the ANN, and 0.3397 for the FL, for removed (MV) dye, and the values of correlation coefficient in the artificial neural network model (ANN), and neuro-fuzzy logic model (FL), were 0.9977 and 0.9121, is shown in Table 5, respectively [31,32].

The summary results relative to parameters of the model, are compared in Table 5. The lowest determination error for removal of the (MV) dye onto *Albizia stem bark Lebbeck* modified by $Fe_2(MoO_4)_3$ nanocomposite in demonstrated process.

3.8. Adsorption isotherms

Considering the variation of equilibrium adsorption capacities in terms of the equilibrium concentration (C_e) of the adsorbate, under the optimum values of other parameters, we can examine some suitable isotherms for representing the respect experimental data [41–43]. Fulfill this goal, we compared the experimental results with the three most common isotherm models, including Langmuir, Freundlich, and Temkin isotherms. The nonlinear form of the model was used for fitting the experimental data (Table 6). The respective equations for these models are as follows:

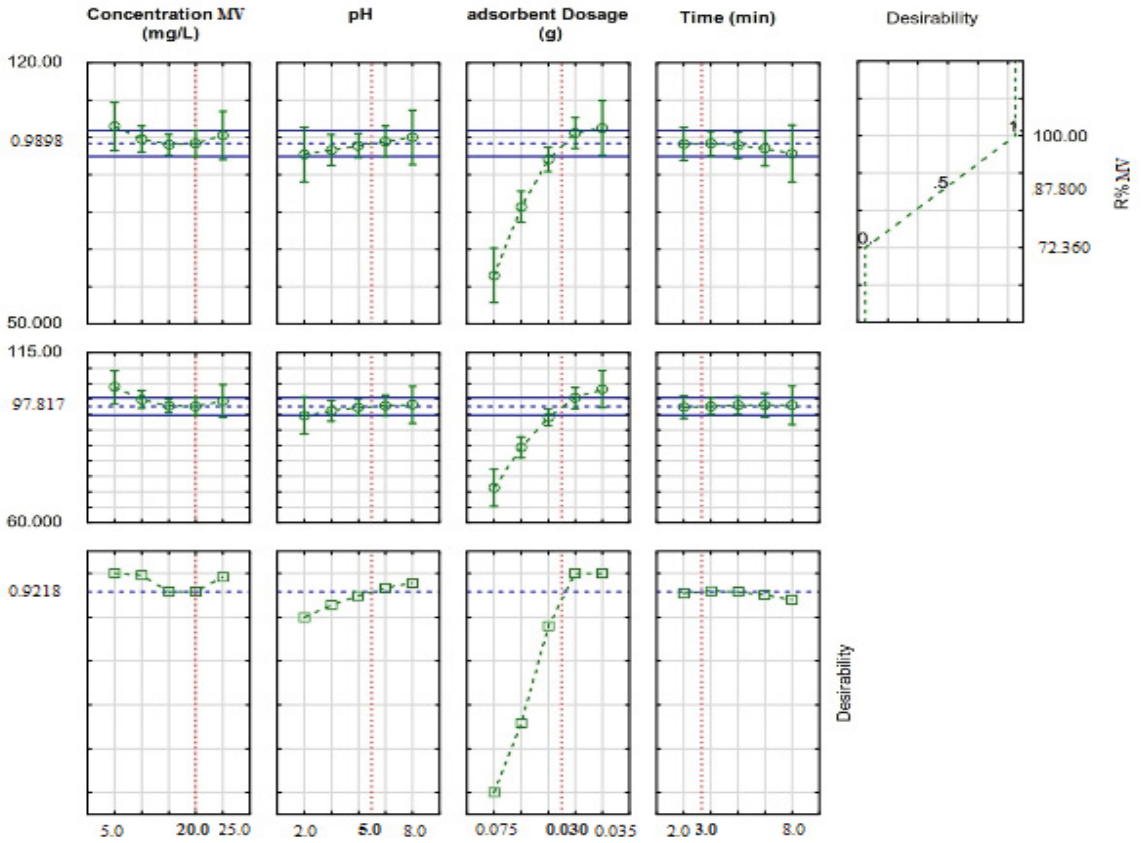

Fig. 9. Profiles values for removal of (MV) dye after optimization.

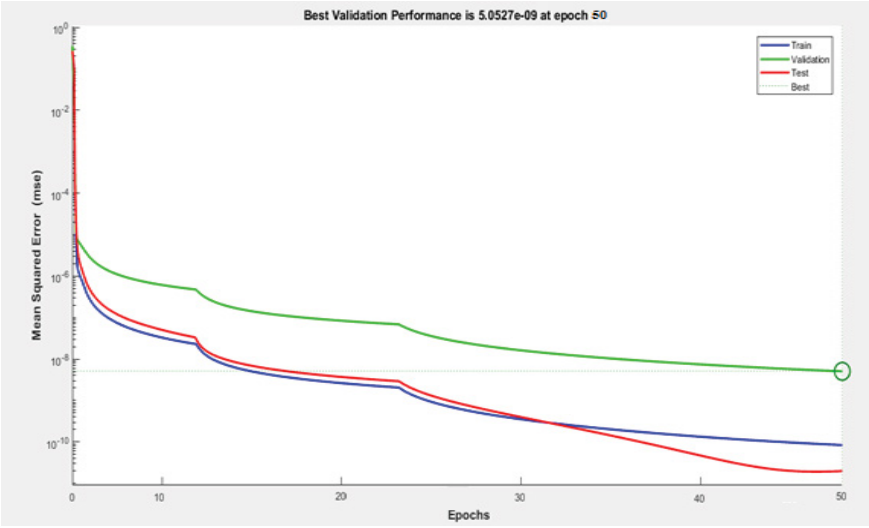

Fig. 10. Evolution of training, validation, and test errors as a function of the number of training epochs during ANNs for the adsorption of the (MV) dye onto *Albizia stem bark Lebbeck* modified by $Fe_2(MoO_4)_3$ nanocomposite.

$$q_e = \frac{q_m K_L C_e}{1 + K_L C_e} \quad \text{Langmuir model} \tag{9}$$

$$q_e = q_m K_F' + C_e^{1/n} \quad \text{Freundlich model} \tag{10}$$

$$q_e = q_m \left(B_T' \ln A_T C_e \right) \quad \text{Temkin model} \tag{11}$$

where q_m represents the maximum value of q_e, which is necessary for the monolayer covering of the whole surface of the used adsorbent. Choose $q_m K_F' = K_F$, the Freundlich

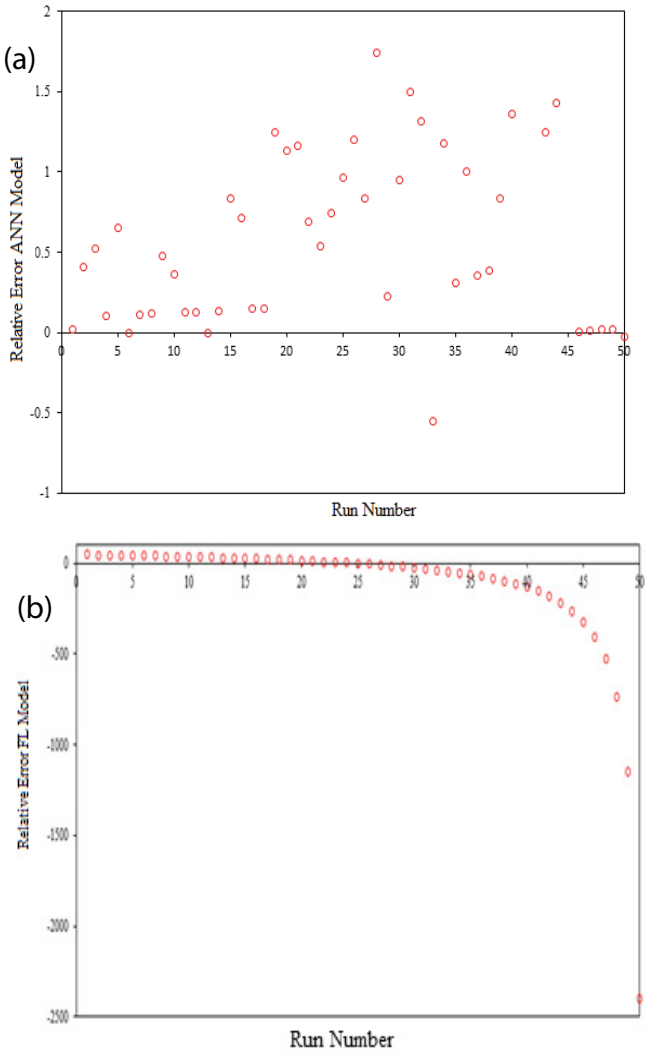

Fig. 11. Comparison of relative error in output data of ANN, and FL models.

Table 5
Statistical comparison of two models, ANN, and FL

Models	SSE	MSE	AARE	SD	R^2
ANN	9.34	0.190	0.03	0.154	0.9977
FL	16.04	0.3397	2.50	44.32	0.9121

model, and $q_m B'_T = B_T$ the Temkin model. The linear equation of the models mentioned above, respectively follows:

$$\frac{1}{q_e} = \frac{1}{q_m K_L C_e} + \frac{1}{q_m} \tag{12}$$

$$\ln q_e = \frac{1}{n} \ln C_e + \ln K_F \tag{13}$$

$$q_e = B_T \ln C_e + B_T \ln A_T \tag{14}$$

Table 6
Adsorption isotherm models of (MV) dye onto *Albizia stem bark Lebbeck* modified by $Fe_2(MoO_4)_3$ nanocomposite

Isotherm	Parameters	*R*% (MV) dye
Langmuir	q_m (mg g^{-1})	120.4
	K_L (L mg^{-1})	0.489
	R^2	0.9899
Freundlich	$1/n$	0.54
	K_F (mg)$^{1-n}$ L^n g^{-1}	4.06
	R^2	0.9805
Temkin	B_T (J mol^{-1})	15.16
	K_T (L mg^{-1})	6.875
	R^2	0.9722

C_0 = 20.0 mg L^{-1}; pH = 5.0; dosage sorbent = 0.03 g; time = 3.0 min; T = 25°C.

3.9. Adsorption kinetics survey

Kinetic models help the evaluate performance of various adsorbents for the removal of dyes. The many kinetic models developed chiefly used are Lagergren's pseudo-first-order kinetics and pseudo-second-order model [44,45].

Quasi-first-order kinetic model formula is:

$$\ln\left(q_e - q_t\right) = \ln q_e - \frac{k_1}{2.303} t \tag{15}$$

Quasi-second-order dynamic model formula is:

$$\frac{t}{q_t} = \frac{1}{k_2 q_e^2} + \frac{t}{q_e} \tag{16}$$

where q_t and q_e are the sorption quantity at time t and equilibrium, respectively, and k is the rate consistent, a plot of t/q via t gives the pseudo-second-order adsorption. Pseudo-second-order rate is constant from the respective fields. From the experimental results, the removal of (MV) dye follows the pseudo-second-order rate shown in Table 7 [45].

3.10. Adsorption thermodynamics

Temperature is one of the most important factors in dye removal efficiency by focusing on changes in the nature of the reactions (exothermic or endothermic) to reveal spontaneous and non-spontaneous reactions, parameters can be used in Eqs. (17) and (18) [45,46].

$$\Delta G^\circ_{\text{ad}} = -RT \ln K_c \tag{17}$$

$$\ln K_c = \frac{\Delta S^\circ_{\text{ad}}}{R} - \frac{\Delta H^\circ_{\text{ad}}}{RT} \tag{18}$$

where T is temperature in Kelvin. Values of the K_C were calculated at 288.0 at 338.0 K temperatures. $\Delta G°$ upon be negative indicating that the studied adsorption process is

spontaneous in the range of used temperature, $\Delta H° < 0$, indicates that the studies adsorption is exothermic. Based on the magnitude of $\Delta H°$, we can say that the mentioned adsorption should be physic sorption one, and van der walls interactions are responsible for adsorption taking place. $\Delta S° < 0$, indicates a decrease in randomness that occurs during (MV) dye adsorption onto *Albizia stem bark Lebbeck* modified by $Fe_2(MoO_4)_3$ nanocomposite, which may come from the (MV) dye aggregation on the *Albizia stem bark Lebbeck* modified by $Fe_2(MoO_4)_3$ nanocomposite surfaces. The results are seen in Table 8 [46,47].

3.11. Adsorption mechanism of (MV) dye into Albizia stem bark Lebbeck modified by $Fe_2(MoO_4)_3$ nanocomposite

The adsorption mechanism of the (MV) dye onto the surface of the *Albizia stem bark Lebbeck* modified by $Fe_2(MoO_4)_3$ nanocomposite can be inferred from the analysis of the Fourier-transform infrared spectroscopy results, in which the presence of functional groups (–O, MoO_4^-, and Fe–O) on the surface was confirmed (Fig. 12), shows the various potential interactions that may occur between the (MV) dye and the *Albizia stem bark Lebbeck* modified by $Fe_2(MoO_4)_3$ nanocomposite surface. Interactions are favored owing to the cationic nature of the dye with the negative surface charges of the *Albizia stem bark Lebbeck* modified by $Fe_2(MoO_4)_3$ nanocomposite. Interactions likely involve hydrogen bonding between the acceptor and the donor groups of the *Albizia stem bark Lebbeck* modified by $Fe_2(MoO_4)_3$ nanocomposite – MV dye [12,36]. With π–π interactions between the p-electron system of the *Albizia stem bark Lebbeck* modified by $Fe_2(MoO_4)_3$ nanocomposite structure and the aromatic rings of the (MV) dye molecules. In neutral and weak alkaline conditions, (MV) dye exhibits substantial proton loss and exists as free ions in the solution, thus inhibiting

Table 7
Various kinetic constants and their correlation coefficients calculated for the adsorption of (MV) dye onto *Albizia stem bark Lebbeck* modified by $Fe_2(MoO_4)_3$ nanocomposite

Models	Parameters	*R*% (MV) dye
Pseudo-first-order kinetic	k_1 (min^{-1})	1.54
	q_e (mg g^{-1})	98.12
	R^2	0.96.08
Pseudo-second-order kinetic	k_2 (min^{-1})	0.507
	q_e (mg g^{-1})	106.6
	R^2	0.9998
q (exp) (mg g^{-1})		51.45

C_0 = 20.0 mg L^{-1}; pH = 5.0; dosage sorbent = 0.03 g; time = 3.0 min; T = 25°C.

Table 8
Thermodynamic parameters for the adsorption of (MV) dye onto *Albizia stem bark Lebbeck* modified by $Fe_2(MoO_4)_3$ nanocomposite

Dye	T (K)	K_C	$\Delta G°$ (kJ mol^{-1})	$\Delta H°$ (kJ mol^{-1})	$\Delta S°$ (kJ mol^{-1} K^{-1})
(MV) dye (20 mg L^{-1})	288	47.5	–9.26	–29.24	–131.49
	308	57.2	–10.36		
	318	96.3	–12.08		
	328	145	–13.57		
	338	291	–15.94		

C_0 = 20.0 mg L^{-1}; pH = 5.0; dosage sorbent = 0.03 g; time = 3.0 min.

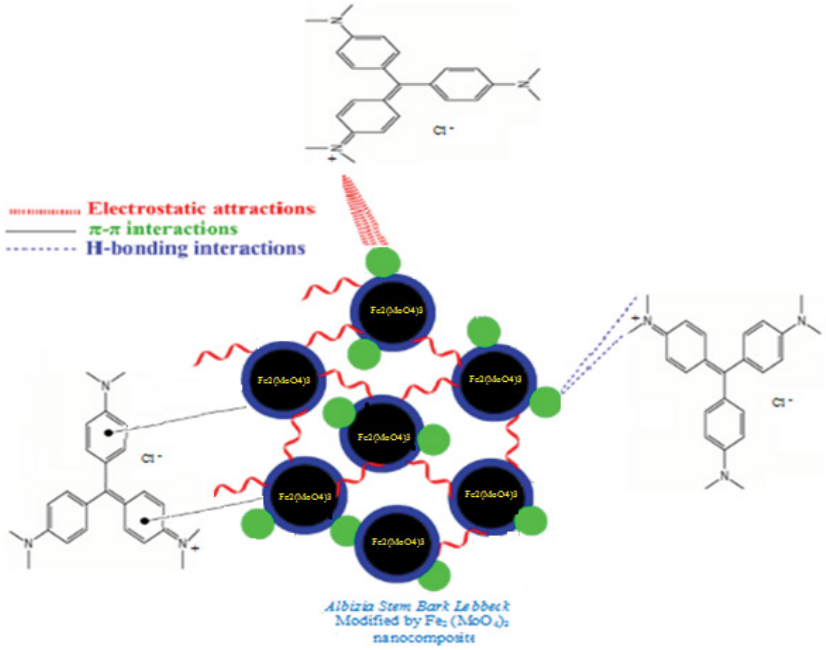

Fig. 12. Illustration of the possible interaction between (MV) dye and surface *Albizia stem bark Lebbeck* modified by $Fe_2(MoO_4)_3$ nanocomposite.

the chemical adsorption to some extent. The structure of *Albizia stem bark Lebbeck* modified by $Fe_2(MoO_4)_3$ nanocomposite, especially after modification, tempers the negative effect *via* physical adsorption [48].

3.12. Effect of solution ionic strength

Most dye wastewaters contain salts, and dye adsorption is strongly influenced by the concentration and nature of these ionic species. The presence of any ion could affect. Selected concentrations of NaCl, in the range of (0.01–1.0 M), were added to individual beakers containing 50 mL of the tested (MV) dye solution (20 mg L^{-1}). The solution pH and *Albizia stem bark Lebbeck* and *Albizia stem bark Lebbeck* modified by $Fe_2(MoO_4)_3$ nanocomposite dosage were fixed at 5.0 and 0.03 g, respectively, and the stirring time was 3.0 min. The mixing time elapsed, for the residual dyes, results indicated that the adsorption *Albizia stem bark Lebbeck* and *Albizia stem bark Lebbeck* modified by $Fe_2(MoO_4)_3$ nanocomposite for (MV) dye were not significantly affected by increasing NaCl concentration. Indicates that Na^+ and Cl^- ions do not compete with the positively or negatively charged groups of the (MV) dye molecules for being adsorbed onto *Albizia stem bark Lebbeck* and *Albizia stem bark Lebbeck* modified by $Fe_2(MoO_4)_3$ nanocomposite. The results seen in (Table 9).

3.13. Recycling of the adsorbent

The ability to recover, and reusing of the adsorbent was tested in several steps of adsorption, and desorption. The result is shown in Fig. 13. As shown in Fig. 13, 98% of (MV) dye was desorbed from the adsorbent after the first cycle, and after 6 cycles, there were slight changes in (MV) dye desorption. So, it was concluded that the desired removal of 98% could be achieved after 6 cycles [29,49].

3.14. Comparison of various adsorbent

A comparison of the maximum adsorption capacities of different adsorbents for the removal of (MV) dye was also reported in Table 10. The outcomes of the table clearly show that the sorption capacity of utilized sorbent in the current study is significantly high, and adsorption capacity, and contact time in this article is superior to other adsorbents

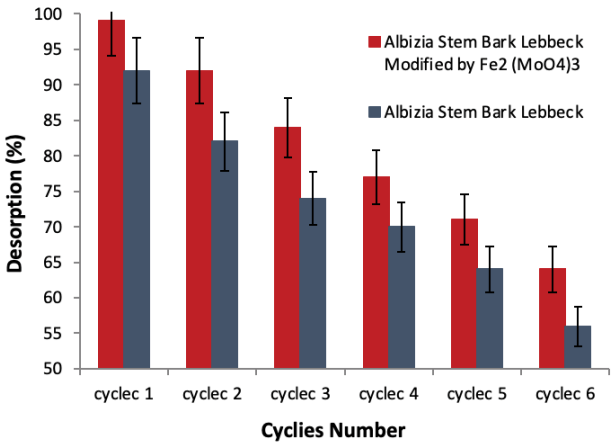

Fig. 13. Desorption of (MV) dye from *Albizia stem bark Lebbeck* modified by $Fe_2(MoO_4)_3$ nanocomposite [C_0 = 20.0 mg L^{-1}; pH = 5.0; dosage sorbent = 0.03 g; time = 3.0 min; T = 25°C].

Table 9
Effect of the ionic strength on the removal of the (MV) dye onto *Albizia stem bark Lebbeck*, and *Albizia stem bark Lebbeck* modified by $Fe_2(MoO_4)_3$ nanocomposite

NaCl (M)	*R*% (MV) dye onto *Albizia stem bark Lebbeck* modified by $Fe_2(MoO_4)_3$ nanocomposite	*R*% (MV) dye onto *Albizia stem bark Lebbeck*
0.00	95.7	79.2
0.02	96.2	79.1
0.04	96.04	79.15
0.06	96.0	79.12
0.08	96.5	79.06
0.1	96.6	79.16
0.2	96.1	79.2
0.4	96.9	79.15
0.6	96.6	79.10
0.8	96.2	79.07
1.0	96.2	79.12

C_0 = 20.0 mg L^{-1}; pH = 5.0; dosage sorbent = 0.03 g; time = 3.0 min; T = 25°C.

Table 10
Comparison of results for this work with other reported

Dye	Adsorbent	Dosage sorbent	pH	Time	Adsorption capacity	References
Methyl violet (MV)	Sawdust/Fe_3O_4 composite	0.28 g	9.0	50 min	46.8 mg g^{-1}	[1]
Methyl violet (MV)	HNT-Fe_3O_4 composite	0.15 g	5.0	10 min	20.04 mg g^{-1}	[6]
Methyl violet (MV)	β-cyclodextrin onto mesoporous silica	0.05 g	6.0	5 min	34.5 mg g^{-1}	[7]
Methyl violet (MV)	Peanut straw char rice	0.5 g	5.0	30 min	101.01, 48.64 and 70.36 mg g^{-1}	[8]
Methyl violet (MV)	*Sanctae-Crucis*	2.0 g	8.0	80 min	10.2 mg g^{-1}	[9]
Methyl violet (MV)	Acid modified activated carbon	0.1 g	7.0	25 min	83.3 mg g^{-1}	[47]
Methyl violet (MV)	*Albizia stem bark Lebbeck* modified by $Fe_2(MoO_4)_3$ nanocomposite	0.03 g	5.0	3 min	120.4 mg g^{-1}	This work

to remove (MV) dye. In general, morphology, particle size and distribution and surface structure of this sorbent were effective in its successful outcomes.

4. Conclusion

In this study, a thorough investigation was performed on the effectiveness of synthesized *Albizia stem bark Lebbeck* modified by $Fe_2(MoO_4)_3$ nanocomposite as an adsorbent for the deletion of (MV) dye from aqueous solutions. In this research, the values of 20 mg L^{-1}, 0.03 g, 5.0, and 3.0 min, the ideal values for (MV) dye concentration, adsorbent mass, pH, and contact time, respectively. Adsorption equilibrium and kinetic data were fitted with the Langmuir monolayer isotherm model (q: 0.9899) and pseudo-second-order kinetics (R^2: 0.999). Thermodynamic parameters ($\Delta G°$: –9.26 kJ mol^{-1}, $\Delta H°$: –29.24 kJ mol^{-1}, $\Delta S°$: –131.49 kJ mol^{-1} K^{-1}) also indicated methyl violet dye adsorption is feasible, spontaneous, and exothermic. The observed outcome the suitability of the artificial neural network model as a tool for mean square error (ANN = 0.190, and FL = 0.3397), for the removal of methyl violet dye. The adsorbent was recyclable more than once and obtained an ideal adsorption capacity (120.4 mg g^{-1}), for methyl violet dye. According to the results, *Albizia stem bark Lebbeck* modified by $Fe_2(MoO_4)_3$ nanocomposite could as a reusable adsorbent, it would be an economically viable option that can lead to aqueous solutions advancement and high-quality treated effluent.

Acknowledgement

The authors gratefully acknowledge support of this work by the Islamic Azad University, Branch of Kermanshah, Iran.

Disclosure statement

No potential conflict of interest was reported by the author(s).

References

[1] H. Pooladi, R. Foroutan, H. Esmaeili, Synthesis of wheat bran sawdust/Fe_3O_4 composite for the removal of methylene blue and methyl violet, Environ. Monit. Assess., 193 (2021) 276, doi: 10.1007/s10661-021-09051-9.
[2] L.P. Lingamdinne, H.R. Koduru, R.R. Karri, A comprehensive review of applications of magnetic graphene oxide based nanocomposites for sustainable water purification, J. Environ. Manage., 231 (2019) 622–634.
[3] M. Pirsaheb, M. Moradi, H.R. Ghaffari, K. Sharafi, Application of response surface methodology for efficiency analysis of strong non-selective ion exchange resin column (A 400 e) in nitrate removal from groundwater, Int. J. Pharm. Technol., 8 (2016) 11023–11034.
[4] T. Tatarchuk, N. Paliychuk, R. Babu Bitra, A. Shyichuk, Mu. Naushad, I. Mironyuk, D. Ziolkovska, Adsorptive removal of toxic Methylene Blue and Acid Orange 7 dyes from aqueous medium using cobalt-zinc ferrite nanoadsorbents, Desal. Water Treat., 150 (2019) 374–385.
[5] Sh. Ghanavati Nasab, A. Semnani, A. Teimouri, H. Kahkesh, T. Momeni Isfahani, S. Habibollahi, Removal of Congo red from aqueous solution by hydroxyapatite nanoparticles loaded on zein as an efficient and green adsorbent: response surface methodology and artificial neural network-genetic algorithm, J. Polym. Environ., 26 (2018) 3677, doi: 10.1007/s10924-018-1246-z.
[6] M.R.R. Kooh, M.K. Dahri, L.B.L. Lim, Removal of the methyl violet 2B dye from aqueous solution using sustainable adsorbent *Artocarpus odoratissimus* stem axis, J. Appl. Water Sci., 7 (2017) 3573–3581.
[7] K. Liu, H. Liu, L. Li, W. Li, J. Liu, T. Tang, Adsorption of methyl violet from aqueous solution using β-cyclodixtrin immobilized onto mesoprous silica, Supramol. Chem., 33 (2021) 1–19.
[8] R.K. Xu, S.C. Xiao, J.H. Yuan, A.Z. Zhao, Adsorption of methyl violet from aqueous solutions by the biochars derived from crop residues, Bioresour. Technol., 102 (2011) 10293–10298.
[9] R. Mahini, H. Esmaeili, H. Foroutan, Adsorption of methyl violet from aqueous solution using brown algae *Padina sanctae-crucis*, Turk. J. Biochem., 24 (2018) 1–12.
[10] A.H. Jawad, N.N.M. Firdaus Hum, A.S. Abdulhameed, M.Z. Mohd Ishak, Mesoporous activated carbon from grass waste via H_3PO_4-activation for methylene blue dye removal: modelling, optimisation, and mechanism study, Int. J. Environ. Anal. Chem., 100 (2020) 1–18.
[11] N.N. Abd Malek, A.H. Jawad, A.S. Abdulhameed, K. Ismail, B.H. Hameed, New magnetic Schiff's base-chitosan-glyoxal/fly ash/Fe_3O_4 biocomposite for the removal of anionic azo dye: an optimized process, Int. J. Biol. Macromol., 146 (2020) 530–539.
[12] A.H. Jawad, A.S. Abdulhameed, S.V. Surip, S. Sabar, Adsorptive performance of carbon modified chitosan biopolymer for cationic dye removal: kinetic, isotherm, thermodynamic, and mechanism study, Int. J. Environ. Anal. Chem., 100 (2020) 1–20, doi: 10.1080/03067319.2020.1807966.
[13] S.H. Ahmadi, P. Davar, A. Manbohi, Adsorptive removal of Reactive Orange 122 from aqueous solutions by ionic liquid coated Fe_3O_4 magnetic nanoparticles as an efficient adsorbent, Iran. J. Chem. Chem. Eng., 35 (2016) 63–73.
[14] A. Dalvand, N. Golchinpoor, S.S. Hosseini, E. Gholibegloo, M.R. Ganjali, M. Khazaei, A.H. Mahvi, H. Kamani, Comparison of *Moringa stenopetala* seed extract as a clean coagulant with alum and *Moringa stenopetala*-alum hybrid coagulant to remove direct dye from textile wastewater, Environ. Sci. Pollut. Res., 23 (2016) 16396–16405.
[15] Sh. Ghanavati Nasab, A. Semnani, A. Teimouri, M. Javaheran Yazd, T. Momeni Isfahani, S. Habibollahi, Decolorization of crystal violet from aqueous solutions by a novel adsorbent chitosan/nanodiopside using response surface methodology and artificial neural network-genetic algorithm, Int. J. Biol. Macromol., 124 (2019) 429–456.
[16] Z. Jafari Harandi, Sh. Ghanavati Nasab, A. Teimouri, Synthesis and characterisation of magnetic activated carbon/diopside nanocomposite for removal of reactive dyes from aqueous solutions: experimental design and optimization, Int. J. Environ. Anal. Chem., 99 (2019) 568–584.
[17] C. Li, S. Farrokhpay, K. Runge, F. Shi, Effect of flotation froth properties on froth rheology, Powder Technol., 287 (2016) 216–255.
[18] M. Abniki, A. Moghimi, Synthesis of chitosan functionalized magnetic carbon nanotubes for dispersive solid-phase extraction of bromocresol green, Micro Nano Lett., 16 (2021) 455–462.
[19] A. Karami, K. Sharafie, K. Karimyan, Sh. Rahimi, R. Davoodi, T. Khosravi, M. Karimaei, M. Miri, H. Sharafi, A. Azari, Application of response surface methodology for statistical analysis, modeling, and optimization of malachite green removal from aqueous solutions by manganese-modified pumice adsorbent, Desal. Water. Treat., 89 (2017) 150–161.
[20] A. Reghioua, D. Barkat, A.H. Jawad, A.S. Abdulhameed, M.R. Khan, Synthesis of Schiff's base magnetic crosslinked chitosan-glyoxal/ZnO/Fe_3O_4 nanoparticles for enhanced adsorption of organic dye: modeling and mechanism study, Sustainable Chem. Pharm., 20 (2021) 100379, doi: 10.1016/j.scp.2021.100379.
[21] A. Reghioua, D. Barkat, A.H. Jawad, A.S. Abdulhameed, A.A. Al-Kahtani, Z.A. ALOthman, Parametric optimization by Box–Behnken design for synthesis of magnetic chitosan-benzil/ZnO/Fe_3O_4 nanocomposite and textile dye removal, J. Environ. Chem. Eng., 9 (2021) 105166, doi: 10.1016/j.jece.2021.105166.

[22] H. Esmaeilli, R. Foroutan, D. Jafari, Effect of interfering ions on phosphate removal from aqueous media using magnesium oxide@ferric molybdate nanocomposite, Korean J. Chem. Eng., 37 (2020) 804–816.
[23] R. Foroutan, S.J. Peighambardoust, S. Hemmati, Preparation of clinoptilolite/starch/$CoFe_2O_4$ magnetic nanocomposite powder and its elimination properties for cationic dyes from water and wastewater, Int. J. Biol. Macromol., 189 (2021) 432–445.
[24] F. Marahel, B. Mombeni Goodajdar, N. Basri, L. Niknam, A. Ghazali, Applying neural network model for adsorption methyl paraben (MP) dye using *Ricinus communis*-capeed Fe_3O_4 NPs synthesized from aqueous solution, Iran. J. Chem. Chem. Eng., 41 (2022) 1–18.
[25] K. Sharafi, M. Pirsaheb, V.K. Gupta, Sh. Agarwal, M. Moradi, Y. Vasseghian, E.N. Dragoi, Phenol adsorption on scoria stone as adsorbent-application of response surface method and artificial neural networks, J. Mol. Liq., 274 (2019) 699–714.
[26] M. Rahmani Piani, M. Abrishamkar, B. Mombeni Goodajdar, M. Hossieni, Trihalomethanes (THMs) removal from aqueous solutions using environmental friendly and effective adsorbent onto *Mespilus germanica* modified by $Fe_2(MoO_4)_3$ nanocomposite on equilibrium, thermodynamic, and kinetics, Desal. Water Treat., 223 (2021) 288–302.
[27] M. Ullah, R. Nazir, M. Khan, W. Khan, M. Shah, S.G. Afridi, The effective removal of heavy metals from water by activated carbon adsorbents of *Albizia lebbeck* and *Melia azedarach* seed shells, J. Soil Water Res., 15 (2020) 30–37.
[28] A. Rafiee, Sh. Ghanavati Nasab, A. Teimouri, Synthesis and characterization of pistachio shell/nanodiopside nanocomposite and its application for removal of Crystal Violet dye from aqueous solutions using central composite design, Int. J. Environ. Anal. Chem., 99 (2019) 1–26.
[29] L. Dos Reis Darcie, B.V. Jacon, G.S. Silva Andrade, A.M. Siqueira Oliveira, M.S. Lopes, T.R. Giraldi, Eucalyptus sawdust as an alternative adsorbent for Rhodamine B dye removal, Desal. Water Treat., 229 (2021) 430–440.
[30] R. Andayesh, M. Abrishamkar, H. Hodaee, Using artificial neural network modeling in predicting the amount of methyl violet dye absorption by modified palm fiber, J. Sci. Islamic Republic Iran, 31 (2020) 221–231.
[31] M. Kiani, S. Bagheri, N. Karachi, E. Alipanahpour Dil, Adsorption of purpurin dye from industrial wastewater using Mn-doped Fe_2O_4 nanoparticles loaded on activated carbon, Desal. Water Treat., 152 (2019) 366–373.
[32] F. Marahel, B. Mombeni Goodajdar, L. Niknam, M. Faridnia, E. Pournamdari, S. Mohammad Doost, Ultrasonic assisted adsorption of methylene blue dye and neural network model for adsorption of methylene blue dye by synthesized Mn-doped PbS nanoparticles, Int. J. Environ. Anal. Chem., 101 (2021) 1–22, doi: 10.1080/03067319.2021.1901895.
[33] H.S. Ghazi Mokri, N. Modirshahla, M.A. Behnajady, B. Vahid, Adsorption of C.I. Acid Red 97 dye from aqueous solution onto walnut shell: kinetics, thermodynamics parameters, isotherms, Int. J. Environ. Sci. Technol., 12 (2015) 1401–1408.
[34] S. Mahdi Hadi, M.K.H. Al-Mashhadani, M.Y. Eisa, Optimization of dye adsorption process for *Albizia lebbeck* pods as a biomass using central composite rotatable design model, Chem. Ind. Chem. Eng. Q., 25 (2019) 39–46.
[35] G.K. Sharma, N. Dubey, Review of shirish (*Albizia lebbeck*) therapeutic properties, Int. J. Ayurvedic Herbal Med., 5 (2015) 1683–1688.
[36] A.H. Jawad, A.S. Abdulhameed, L.D. Wilson, S.S.A. Syed-Hassan, Z.A. ALOthman, M. Rizwan Khan, High surface area and mesoporous activated carbon from KOH-activated dragon fruit peels for methylene blue dye adsorption: optimization and mechanism study, Chin. J. Chem. Eng., 32 (2021) 281–290.
[37] F. Mohammadi, A. Esrafili, H.R. Sobhi, M. Behbahani, M. Kermani, E. Asgari, Z. Rostami Fasih, Evaluation of adsorption and removal of methylparaben from aqueous solutions using amino-functionalized magnetic nanoparticles as an efficient adsorbent: optimization and modeling by response surface methodology (RSM), Desal. Water Treat., 103 (2018) 248–260.
[38] M. Pargari, F. Marahel, B. Mombini Godajdar, Ultrasonic assisted adsorption of propyl paraben on uultrasonically synthesized TiO_2 nanoparticles loaded on activated carbon: optimization, kinetic and equilibrium studies, Desal. Water Treat., 212 (2021) 164–172.
[39] M. Kiani, S. Bagheri, A. Khalaji, N. Karachi, Ultrasonic supported deletion of Rhodamine B on ultrasonically synthesized zinc hydroxide nanoparticles on activated carbon concocted from wood of cherry tree: experimental design methodology and artificial neural network, Desal. Water Treat., 226 (2021) 147–156.
[40] S. Hajati, M. Ghaedi, B. Barazesh, F. Karimi, R. Sahraei, A. Daneshfar, A. Asghari, Application of high order derivative spectrophotometry to resolve the spectra overlap between BG and MB for the simultaneous determination of them: ruthenium nanoparticle loaded activated carbon as adsorbent, J. Ind. Eng. Chem., 20 (2014) 2421–2427.
[41] L. Daneshvar, A. Nezamzadeh-Ejhieh, Photocatalytic activity of ZnO nanoparticles towards tinidazole degradation: experimental design by response surface methodology (RSM), Desal. Water Treat., 141 (2019) 364–376.
[42] Y. Yang, Y. Xie, L. Pang, M. Li, X. Song, J. Wen, H. Zhao, Preparation of reduced graphene oxide/poly(acrylamide) nanocomposite and its adsorption of Pb^{2+} and methylene blue, Langmuir, 29 (2013) 10727–10736.
[43] F. Maghami, M. Abrishamkar, B. Mombeni Goodajdar, M. Hossieni, Simultaneous adsorption of methylparaben and propylparaben dyes from aqueous solution using synthesized *Albizia lebbeck* leaves-capped silver nanoparticles, Desal. Water Treat., 223 (2021) 388–392.
[44] M. Hubbe, S. Azizian, S. Douven, Implications of apparent pseudo-second-order adsorption kinetics onto cellulosic materials: a review, BioResources, 14 (2019) 7582–7626.
[45] A. Asfaram, M. Ghaedi, S. Hajati, A. Goudarzi, Synthesis of magnetic γ-Fe_2O_3-based nanomaterial for ultrasonic assisted dyes adsorption: modeling and optimization, Ultrason. Sonochem., 32 (2016) 418–431.
[46] F. Marahel, Adsorption of hazardous methylene green dye from aqueous solution onto tin sulfide nanoparticles loaded activated carbon: isotherm and kinetics study, Iran. J. Chem. Chem. Eng., 38 (2019) 129–142.
[47] A.T.M. Din, B.H. Hameed, Adsorption of methyl violet dye on acid modified activated carbon: isotherms and thermodynamics, J. Appl. Sci. Environ. Sanitation, 5 (2010) 161–170.
[48] A.S. Abdulhameed, N.N.M. Firdaus Hum, S. Rangabhashiyam, A.H. Jawad, L.D.Z. Wilson, M. Yaseen, A.A. Al-Kahtani, Z.A. ALOthman, Statistical modeling and mechanistic pathway for methylene blue dye removal by high surface area and mesoporous grass-based activated carbon using K_2CO_3 activator, J. Environ. Chem. Eng., 9 (2021) 105530, doi: 10.1016/j.jece.2021.105530.
[49] Sh. Bouroumand, F. Marahel, F. Khazali, Removal of Yellow HE_4G dye from aqueous solutions using synthesized Mn-doped PbS (PbS:Mn) nanoparticles, Desal. Water Treat., 223 (2021) 388–392.